Potassium Difluorophosphate as an Electrolyte Additive for Potassium Ion Batteries

Huan Yang,[a] *Chih-Yao Chen,*[b] *Jinkwang Hwang,*[a] *Keigo Kubota,*[b]

Kazuhiko Matsumoto,[a, b, c,*] *Rika Hagiwara*[a, b, c]

[a] Graduate School of Energy Science, Kyoto University, Sakyo-ku, Kyoto 606-8501, Japan

[b] AIST-Kyoto University Chemical Energy Materials Open Innovation Laboratory (ChEM-OIL), National Institute of Advanced Industrial Science and Technology (AIST), Sakyo-ku, Kyoto 606-8501, Japan

[c] Unit of Elements Strategy Initiative for Catalysts & Batteries (ESICB), Kyoto University, Katsura, Kyoto 615-8510, Japan

[*]Corresponding author:

E-mail: k-matsumoto@energy.kyoto-u.ac.jp

Abstract

The limited cyclability and inferior Coulombic efficiency of graphite negative electrodes have been major impediments to their practical utilization in potassium-ion batteries (PIBs). Herein, for the first time, potassium difluorophosphate (KDFP) electrolyte additive is demonstrated as a viable solution to these bottlenecks by facilitating the formation of a stable and K^+-conducting solid-electrolyte interphase (SEI) on graphite. The addition of 0.2 wt% KDFP to the electrolyte, results in significant improvements on the (de)potassiation kinetics, capacity retention (76.8% after 400 cycles with KDFP vs. 27.4% after 100 cycles without KDFP) as well as average Coulombic efficiency (~99.9 % during 400 cycles) of graphite electrode. Moreover, the KDFP-containing electrolyte also enables durable cycling of the K/K symmetric cell at higher efficiencies and lower interfacial resistance as opposed to the electrolyte without KDFP. X-ray diffraction and Raman spectroscopy analyses have confirmed the reversible formation of a phase-pure stage-1 potassium-graphite intercalation compound (KC_8) with the aid of KDFP. The enhanced electrochemical performance by the KDFP addition is discussed based on the analysis of the SEI layer on graphite and K metal electrodes by X-ray photoelectron spectroscopy.

Keywords: Potassium difluorophosphate (KDFP), Electrolyte additive, Potassium-ion batteries, Graphite, Graphite intercalation compounds (GICs).

1. Introduction

Recent growth in environmental sensitivity has spurred unprecedented innovations in renewable energy, most notably, solar and wind power. To address the intermittency of these alternative power sources, energy storage devices such as rechargeable batteries are used to optimize power supply. For this reason, Lithium-ion battery (LIB) technology has been growing expeditiously over the years. However, rising costs and rapidly depleting lithium resources have aroused doubts in its sustainability for future energy storage.[1]

In this context, sodium-ion batteries (SIBs) and potassium-ion batteries (PIBs) have emerged as successors owing to their abundance in nature, low cost, and widespread geographical distribution of sodium and potassium resources.[2-4] Particularly, PIBs have shown great electrochemical performance revealing their potential as LIB replacements. The redox potential of K^+/K (–2.93 V vs. standard hydrogen electrode) is lower than that of Na^+/Na (–2.71 V) and still very close to that of Li^+/Li (–3.04 V). This demonstrates prospects of a battery with a competitive energy density and high voltage operation capabilities.[5-10] Although K^+ has a larger ionic radius of 1.38 Å compared to Li^+ (0.76 Å) and Na^+ (1.02 Å), it has the smallest Stokes radius in certain solvents due to the weaker Lewis acidity, which is favorable to the transport behavior within the electrolyte and charge transfer at the electrolyte-electrode interface for PIBs.[11-12]

Besides the excellent electrochemistry of K, the compatibility of well-established LIB components such as graphite negative electrodes in PIBs has also stimulated their advancement.[13] Graphite has been the principle choice for negative electrodes for its ability to store cations, forming graphite intercalation compounds (GICs). Even so, these negative electrodes cannot be adopted in SIBs since only a limited amount of Na^+ (< 40 mAh g^{-1}) can be stored within the graphitic layers. This is

generally ascribed to the thermodynamic instability of Na–GICs,[14-15] unless a solvent is cointercalated between two layers.[16-17] On the other hand, K-GICs possess a rich variety of phases over a wide range of K stoichiometry, making them suitable for battery operations. Just like in the Li intercalation process, the structural properties of the K-GIC is dependent on the amount of K intercalants present in the graphitic layers at each stage.[4, 18-20]

The staging mechanism of K-GICs consists of a sequential formation of KC_{60} (stage-5), KC_{48} (stage-4), KC_{36} (stage-3), KC_{24} (stage-2), and KC_8 (stage-1).[21] Formation of the KC_8 (stage-1 K-GIC) provides a theoretical capacity of 279 $mAhg^{-1}$.[22] Although previous works have reported the formation of phase-pure KC_8 under specific conditions,[23-24] it is worth noting that the "fully" charged state of graphite is usually accompanied by the residual KC_{24} (stage-2 K-GIC) which remarkably diminishes the practically attainable capacity.[4, 6, 12, 25] The incomplete potassiation is generally attributed to the ineffectiveness of solid electrolyte-interphase (SEI) formed at the electrode surface in preventing continuous decomposition of the electrolyte, which eventually leads to excessive SEI buildup and large cell impedance.[26] Since the quantity of the SEI is determined by the electrolyte,[27] the selection and optimization of electrolytes are critical in harnessing the high performance of graphite anodes in PIBs.

To tackle this issue, different approaches have been taken to develop advanced electrolytes for PIB operations. For instance, concentrated electrolyte ($K[N(SO_2F)_2]$:ethyl methyl carbonate with a molar ratio of 1:2.5) has been used to facilitate the formation of a robust inorganic SEI on the graphite surface.[23] There have also been attempts to optimize the solvent formulation to reduce the growth rate of SEI.[25] In commercialized LIBs, incorporating various types of additives is considered an effective and economical way to optimize battery performance.[28-31] Difluorophosphate salts have been found to have good film-forming properties and are often effective in obtaining satisfactory electrochemical

performance in LIBs. Introduction of a small amount (< 2 wt%) of lithium difluorophosphate (LiDFP), which is an intermediate decomposition product of $LiPF_6$, into the electrolyte has been proven beneficial in (i) inhibiting the hydrolysis of $LiPF_6$ and restraining the generation of HPO_2F_2[32-34] and (ii) forming a more ionically conductive surface film on graphite. Consequently, graphite electrodes in the LiDFP-containing batteries show fast Li^+ ion storage/release kinetics and good rate and cycling capability.[35] Despite the significant progress of electrolyte additives in LIBs, the functionality of their analogs in PIBs remains vastly underexplored.

In this study, the effects of the potassium difluorophosphate (KDFP) additive in a KPF_6-based organic electrolyte have been investigated. A three-electrode cell with a Pt or Al working electrode were used to analyze the basic electrochemical stability of the electrolytes with and without KDFP. Potassium deposition/dissolution was evaluated using K/Al cells and K/K symmetric cells, and subsequent analysis of interfacial behavior was performed through electrochemical impedance spectroscopy (EIS). The potassiation/depotassiation processes of the graphite electrode were confirmed by X-ray diffraction (XRD) and Raman spectroscopy. The morphologies of graphite electrodes were observed by fieldemission scanning electron microscopy (FE-SEM, Hitachi SU-8020). Additionally, in order to understand the improved electrochemical properties, X-ray photoelectron spectroscopy (XPS) was also performed to examine the different SEI components in the electrolyte with KDFP. The results were compared with a commonly used film-forming additive fluoroethylene carbonate (FEC) under the same conditions. This work has also employed galvanostatic intermittent titration technique (GITT), rate capability, and cycle tests to provide a comprehensive electrochemical evaluation of the graphite electrode.

2. Experimental Section

2.1. Materials and preparation of electrodes.

KPO_3 and KPF_6 (Aldrich, purity > 99%) were vacuum-dried at 80 °C for 24 h before use. KDFP was synthesized through the reaction of KPO_3 and KPF_6 in the molar ratio of 2:1 at 320 °C in a platinum crucible over three days.[36] The purity of the as-prepared KDFP was confirmed by X-ray powder diffraction (**Figure S1**). Moisture- and air-sensitive materials were handled in a glove box (Miwa Manufacturing Co., Ltd.) under dry deoxygenated Ar gas. The dew point (below –80 °C) and oxygen content (below 1 ppm), monitored using Oxygen Analyzer (DF-150E, General Electric Company). Electrode materials and reagents were weighed using an electric balance (CPA225D, Sartorius; WMC25-SH, Mettler Toledo) in the glove box. The as-prepared KDFP powder was weighed to the target weight ratio and added into 0.5 M KPF_6 in ethylene carbonate and diethylene carbonate (EC/DEC, in a 1:1 volume ratio, Kishida Chemical Co., Ltd., >99.0 % purity, water content < 10 ppm) and continuously stirred for 1 day in an Ar-filled glovebox until uniformity was achieved. Graphite electrodes were prepared by mixing graphite as an active material (particle size of 10 μm in averate SNO-10, SEC Carbon) with carbon black, carboxyl methylcellulose (CMC), and styrene-butadiene rubber (SBR) at a weight ratio of 80:10:5:5 in *N*-methylpyrrolidone by a solid/liquid ratio of 0.51. The slurry was then pasted onto Cu foil and vacuum-dried at 333 K overnight. The electrodes with 10 mm diameter were punched out from the foil and the electrodes were vacuum-dried at 383 K for 10 h before cell assembly. The average mass loading and density of the prepared graphite electrodes were 1.3 mg cm^{-2} and 0.7 g cm^{-3}, respectively. The amount of electrolyte in a coin cell was typically 0.1 cm^3. Potassium metal (Kojundo Chemical Laboratory, purity 99.5%) was pressed onto an Al current collector and used as the counter electrode.

2.2. Characterization.

Cyclic voltammetry was carried out using a conventional three-electrode cell configuration under argon atmosphere at 25 °C with an Al or Pt working electrode, a Pt wire counter electrode, and an Ag^+/Ag reference electrode. The reference electrode consisted of silver wire immersed in 0.05 mol kg^{-1} $AgSO_3CF_3$/electrolyte solution (0.5 M KPF_6-EC/DEC (1:1, v:v) with or without additive) filled in a glass tube with porous frit. The electrode potential in the three-electrode tests was converted to the K^+/K standard based on the experimentally determined K^+/K potential (–3.83 V vs. Ag^+/Ag, see **Figure. S2**). The electrode potential was controlled and recorded by a potentiostat (Hokuto Denko Co., Ltd., HZ-5000). The efficiency of K metal deposition/dissolution was measured in 2032-type coin cells with a Cu plate working electrode (10 mm diameter, 0.2 mm thickness) and a K metal counter electrode. The K/K symmetric cells were assembled for electrochemical impedance and polarization tests with K metal on both sides of the cell. A glass fiber filter (Whatman, GF/A, thickness 260 μm) was used as the separator. Charge/discharge measurements were performed in a K/graphite half-cell using a charge-discharge unit (Hokuto Denko, HJ1001SD8) after resting for 1 h. Rate capability was tested at constant rates in the sequence of C/20, C/10, C/5, C/2, 1C, and C/20 (where 1 C corresponds to a current density of 279 mA g^{-1} based on the theoretical capacity of KC_8) within a voltage range of 0.001–2.5 V. Cycling tests were performed at a constant rate of C/3 in the same voltage range as the rate capability test. Galvanostatic intermittent titration technique (GITT) measurement was measured by applying a constant rate of C/20 for 30 min, followed by voltage relaxation for 2 h. The electrolytes utilized in the aforementioned electrochemical measurements were 0.5 M KPF_6-EC/DEC (1:1, v:v) with 0 wt%, 0.1 wt%, and 0.2 wt% KDFP additive. The 0.5 M KPF_6-EC/DEC (1:1, v:v) electrolytes with 0.3 wt% and 3 wt% FEC additives were also examined in the same condition for comparison. Ionic conductivity of the electrolyte was measured by an AC impedance technique using a 3532-80 impedance analyzer (Hioki E.E. Corp.). Samples were sealed in a T-shaped cell with two stainless steel electrodes in the glove box and placed in a temperature-controlled thermostatic chamber (SU-242, ESPEC). The density

of all the studied electrolytes was measured with an oscillating U-tube density meter (DMA 4500 M, Anton Paar GmbH).

X-ray diffraction patterns were recorded in the Bragg-Brentano geometry using a Rigaku Smart Lab diffractometer with Cu-*K*α radiation (40 kV and 30 mA). The samples for the XRD measurements were set in an airtight cell under a dry argon atmosphere. Raman spectra were collected by DXR3 Smart Raman (Thermo Fisher Scientific) using a 532 nm diode-pumped solid-state laser for fresh and (de)potassiated graphite electrodes. The samples for Raman spectroscopy were sealed in a glass cell and isolated from the air. The SEI layer components were analyzed using *ex-situ* XPS (JEOL, JPS-9030, Mg *K*α source). The electrodes samples for XPS were washed with EC/DMC and dried at 25 °C under vacuum overnight and an airtight transfer vessel was used for tranfering the sample into the XPS machine.

3. Results and Discussion

3.1. Electrochemical stability of the electrolyte

In the preliminary test to ascertain the solubility of KDFP in 0.5 M KPF_6-EC/DEC, saturation of the additive was found to occur between concentrations of 0.2 and 0.3 wt%. Subsequently, 0.5 M KPF_6-EC/DEC electrolyte containing 0 wt%, 0.1 wt%, and 0.2 wt% KDFP were used in the assembly of three-electrode cells using Pt (anodic side) and Al (anodic and cathodic sides) working electrodes. To assess the electrochemical behavior of the electrodes in the electrolyte, cyclic voltammetry was performed at 25 °C. As illustrated in **Figure 1**, cyclic voltammograms obtained on the Pt electrode in 0.5 M KPF_6 EC/DEC with 0 wt% KDFP demonstrated a relatively low anodic potential limit of 4.40 V vs. K^+/K attained at a current density of 0.1 mA cm^{-2}. Higher anodic potential limits of 5.26 V and 5.42 V are observed in electrolyte with 0.1 wt% KDFP and 0.2 wt% KDFP, respectively. Previous reports on difluorophosphate additives (specifically LiDFP in $LiPF_6$-based electrolytes) have suggested that the addition of KDFP suppresses the generation of hydrolysis products (mainly HPO_2F_2), expanding the electrochemical stability window of the electrolyte[32, 37]. For comparison, as shown in **Figure S3**, the addition of 0.3 wt% and 3 wt% FEC also improves the anodic potential limit to 5.22 and 5.48 V, respectively compared to the case without additive. The negligible current (less than 1 μA cm^{-2} at 6.43 V vs. K^+/K) acquired on the Al electrode during anodic scan proves the compatibility of Al as a current collector owing to the passivation layer on Al regardless of the addition of additives.[38]

Cathodic scans were thereafter performed on the Al electrode in the selected 0.5 M KPF_6-EC/DEC electrolytes (**Figure 1b**). In the case of 0 wt% KDFP electrolyte, a current corresponding to K metal deposition was seen to occur from –0.4 V vs. K^+/K, shortly followed by K metal dissolution around 0 V vs. K^+/K upon the anodic scan. It is noted that the corresponding Coulombic efficiency of K

deposition/dissolution in the cyclic voltammograms increases from 5% in 0 wt% KDFP electrolyte to 31 % and 40% in the 0.1 wt% KDFP and 0.2 wt% KDFP, respectively. Comparably as shown in **Figure S3**, a similar pattern is observed with respect to FEC additives where Coulombic efficiencies of 26% and 33% are noted in 0.3 wt% FEC and 3wt% FEC electrolytes, respectively. This suggests that FEC additives are not as effective as KDFP.

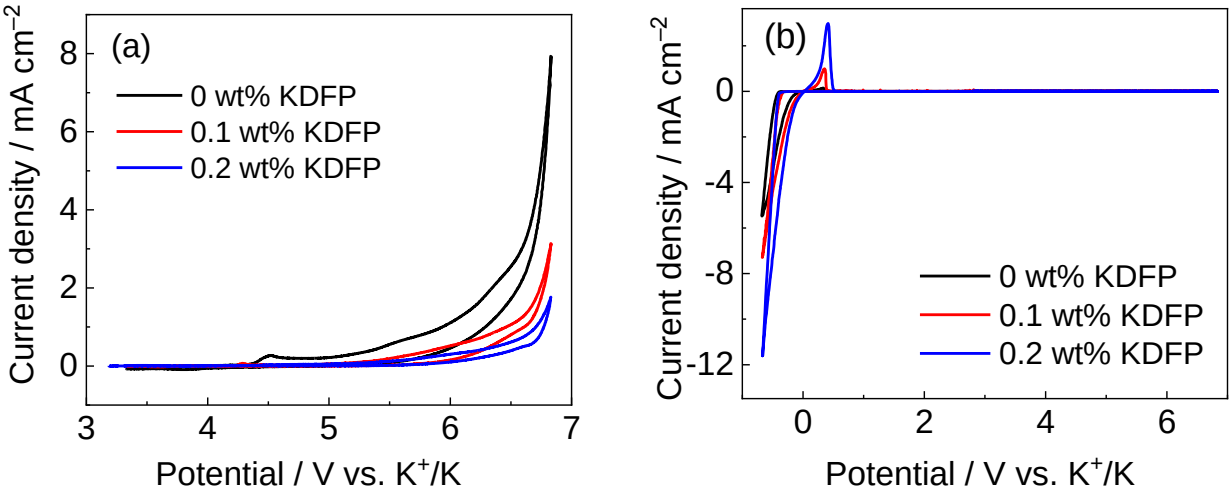

Figure 1. Cyclic voltammograms of (a) Pt (anodic side) and (b) Al (anodic and cathodic sides) electrodes in 0.5 M KPF_6-EC/DEC with varying weight ratios of KDFP additive. Scan rate: 5 mV s^{-1}. See **Figure S3** for cyclic voltammograms of 0.5 M KPF_6-EC/DEC with FEC additive.

3.2. K metal deposition/dissolution behavior and interfacial properties

The Coulombic efficiency (ε_{cycle}) of K metal deposition/dissolution on a Cu plate working electrode assembled alongside the K metal counter electrode in a coin cell was derived. The ε_{cycle} was calculated in accordance with **Eq. (1)**:[39]

$$\varepsilon_{cycle} = N_{eff} \cdot Q_{cycle} / (Qex + N_{eff} \cdot Q_{cycle}) \quad (1)$$

where N_{eff} is the total number of cycles until the electrode potential reaches 0.5 V vs. K^+/K, Q_{cycle} is the electric charge for deposition/dissolution (0.02 C cm^{-2}) in each cycle and Q_{ex} is the electric charge for pre-deposition (0.1 C cm^{-2}) in the first step before cycling. As illustrated in **Figure S4**, voltage profiles of the electrodes in 0.5 M KPF_6-EC/DEC electrolytes containing varying weight ratios of KDFP and FEC were obtained at 25 °C. The results indicate a gradual improvement of the ε_{cycle} with increasing concentrations of KDFP or FEC additives, confirming the favorable effect of additives on SEI formation on K metal surface. However, the larger polarization is observed in the case of FEC-added electrolytes, suggesting the different SEI nature.

The compatibility of K metal electrodes in the electrolytes containing varying weight ratios of KDFP was further evaluated in K/K symmetric cells to exclude the effect from the counter K electrode.[40-41] The symmetric cells were cycled in each electrolyte at current densities in the sequence of 10, 50, 100, and 500 μA cm^{-2} for 10 cycles. Each cycle consisted of 8-min deposition and 8-min dissolution with a 2-min rest in between. The resulting voltage profiles during the galvanostatic K metal deposition/dissolution tests are shown in **Figure 2**. As shown in **Figure 2a**, the overpotential of 55 mV observed in the 0 wt% KDFP electrolyte at 10 μA cm^{-2} significantly increases with increasing current densities. On the other hand, the overpotentials observed at 10 μA cm^{-2} significantly decrease with increasing concentrations of KDFP (*i.e.* 17 mV and 15 mV for 0.1 wt% KDFP and 0.2 wt% KDFP, respectively). Considering the similar ionic conductivities of these electrolytes (see **Figure S5** for temperature dependence of ionic conductivities), the major reason for the lower overpotential exhibited in the electrolytes with KDFP could primarily be attributed to reduced interfacial resistance through

the SEI film (see also **Figure S5** for temperature dependence of density).[41-42] Previous studies of the electrolytes for LIB have reported similar improvements in the interfacial properties of the ionically conductive SEI components formed in electrolytes with LiDFP additives.[33, 35] Similar SEI components in the case of KDFP additives are also confirmed in XPS results as will be discussed in a later section. For comparison, the results acquired in the electrolyte with 0.3 wt% and 3 wt% FEC are shown in **Figure S6**. Evidently, compared to electrolytes with KDFP, the overall overpotential is greater and dramatically increases with increasing current density in electrolytes with FEC (15 mV for 0.2 wt% KDFP vs.138 mV for 0.3 wt% FEC, respectively, at 10 μA cm^{-2}). These results could be associated with a more resistive SEI derived from FEC-derived products. Furthermore, the observations made with K/K symmetric cells are in conformance with the deposition/dissolution tests performed on the K/Cu cells. It is also noteworthy that, the shape of voltage profiles in each cycle is steady with less polarization and stable from the early stage during the cycles with KDFP, whereas neat and FEC electrolyte required prolonged time to be stabilized.

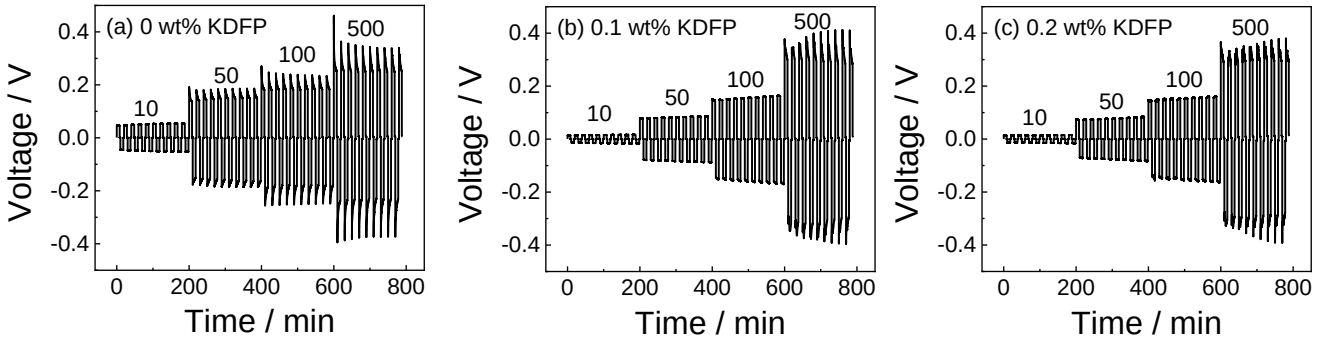

Figure 2. Voltage profiles of the K/K symmetrical cells during galvanostatic K metal deposition/dissolution in 0.5 M KPF_6-EC/DEC with (a) 0 wt%, (b) 0.1 wt%, and (c) 0.2 wt% KFDP additives at 25 °C. The numbers shown in each panel denote current densities in μA cm^{-2} (see **Figure S6** for the voltage profiles of the cases with FEC additive)

To investigate the interfacial behavior of the SEI formed, EIS analysis was performed on the K/K symmetric cells after the formation of a stable SEI layer, which was achieved by cycling the cells at 10 μA cm^{-2} for 8 min over the course of three cycles. **Figure 3d** illustrates a schematic of the equivalent circuit used for this analysis. The resulting electrolyte resistance R_{bulk} and interfacial resistances R_{int} resistances are listed in **Table S1**. The time-evolving EIS results (**Figure 3a-c**) illustrate that the R_{bulk} values remain low regardless of the amount of additive present; consistent with the ionic conductivity results shown in **Figure S5**. However, a dramatic decrease in the R_{int} values is manifested in the presence of KDFP, signifying that a stabilized interface is formed on the K. These results conform to the voltage profiles of the K/K symmetric cells shown in **Figure 2**. In the case of the FEC additive, as shown in **Figure S7** and **Table S1**, a progressive increase of R_{int} is observed in the presence of the additive, which verifies the inferior stability of the SEI formed. For the cells evaluated after storage for 5 days, the R_{int} value is more than ten times larger than that in the presence of KDFP.

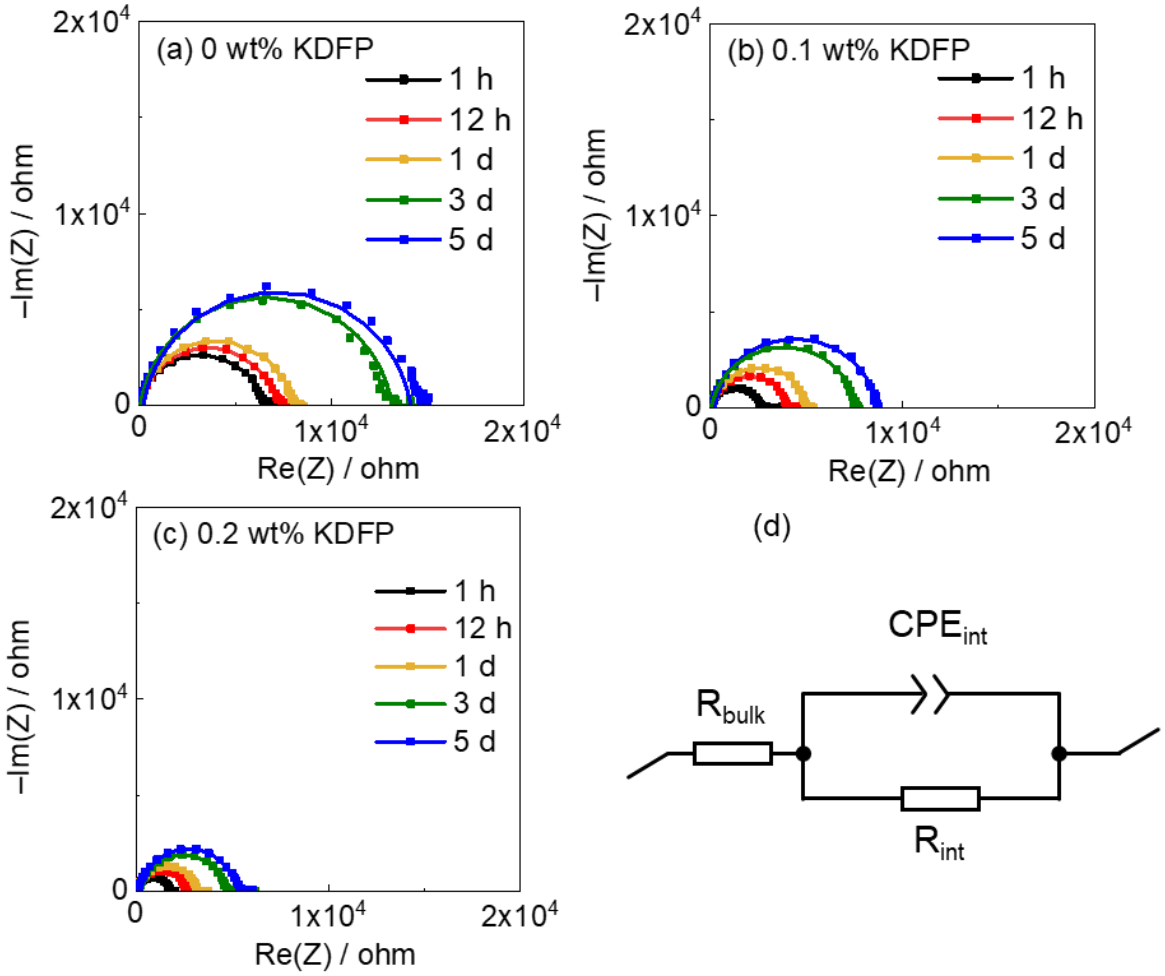

Figure 3. Nyquist plots and fitting lines of the K/K symmetric cells at 25 °C using the 0.5 M KPF_6-EC/DEC electrolyte with (a) 0 wt%, (b) 0.1 wt%, and (c) 0.2 wt% KDFP in the frequency range of 100 kHz−10 mHz. (d) Equivalent circuit used for data fitting. AC amplitude: 10 mV. (See **Figure S7** for the Nyquist plots and fitting lines of the cases with FEC additive.)

3.3. The Effect of KDFP on the electrochemical behavior of graphite

To assess the effect of KDFP on the electrochemical behavior of graphite, cyclic voltammetry profiles of the graphite electrode in electrolytes with varying amounts of KDFP were measured in a three-electrode cell at a scan rate of 5 mV s^{-1} between OCP and 0.01 V vs. K^+/K as shown in **Figure S8**. For the additive-free electrolyte, the CV curve shows a pair of redox peaks centered at ca. 0.02 V

vs. K^+/K; an indication of the potassium intercalation/deintercalation into/from graphite. The relatively low initial Coulombic efficiency (36%) achieved from the 0 wt% KDFP electrolyte is ascribed to the severe reductive decomposition of the electrolyte without an additive, as discussed above. In the case of electrolytes with 0.1 wt% and 0.2 wt% KDFP, a significant increase in the current density is observed; which corresponds to the facile interfacial reaction. Moreover, a new reduction peak which appears at 0.6 V vs. K^+/K, depicts the reductive decomposition of KDFP. It is crucial to note that the initial Coulombic efficiency is remarkably improved to 64% (0.1 wt% KDFP) and 75% (0.2 wt% KDFP) despite the additional SEI created from KDFP decomposition. The higher Coulombic efficiency is most likely due to the preferential reduction of KDFP into a stable SEI layer on the graphite surface that suppresses the decomposition of other electrolyte components[33, 35]. This favorable initial SEI formation is postulated to facilitate the subsequent K intercalation/deintercalation into/from graphite. From **Figure S8d**, reduction of FEC is identifiable at the higher potentials of 1.3 and 1.0 V vs K^+/K compared to the case without FEC, however, only a limited improvement in Coulombic efficiency is obtained (41%).

The K^+ intercalation/deintercalation behavior into/from graphite is examined by K/graphite half-cells. In the present study, intercalation and deintercalation of K^+ are defined as charge and discharge, respectively. **Figure 4** shows the initial three charge-discharge curves measured at C/20 (1C = 279 mA g^{-1}) and the corresponding dQ/dV plots. For the additive-free electrolyte, the charge curve consists of two regions. The first region slopes in the range of 0.4 and 0.2 V and the second is a voltage plateau at 0.15 V[25]. During the first charge, a charge capacity of 309 mAh g^{-1} was achieved in total (**Figure 4a**). Besides, a small irreversible reduction peak, which is related to the decomposition of the electrolyte during the formation of SEI, was observed at 0.29 V (**Figure 4d**). Three subsequent peaks

corresponding to the phase transformation process to KC_{36}, KC_{24}, and KC_8 were also attained at 0.26, 0.20, and 0.15 V, respectively, in accordance with the previous study.[23] This is accompanied by a conspicuous change in the color of the graphite electrode from grey to gold, proving the formation of KC_8 (**Figure S9**).[4, 25] During the discharge process, the peaks observed at 0.28, 0.37, and 0.49 V in the dQ/dV plot correspond to the depotassiation steps of K-GICs (see **Table S2** for voltage details).[23] A first discharge capacity of 266 mAh g^{-1} (**Figure 4a**) is attained with a resultant initial Coulombic efficiency of 84.5%. As shown in **Figure S9**, the appearance of the depotassiated electrode returns to dark grey, supporting the complete depotassiation of graphite.

In the presence of KDFP, relatively large reductive peaks emerged at ca. 0.36 V, indicating additional reduction associated with SEI formation, as had been portrayed earlier by the cyclic voltammetry results. The first discharge capacity of 273 and 274 mAh g^{-1} was obtained from 0.1 wt% and 0.2 wt% KDFP electrolytes, respectively, which is fairly close to the theoretical capacity of 279 mAh g^{-1} for fully intercalated KC_8. Compared to the electrolyte without additives, slightly higher initial Coulombic efficiency of 86.1% and 86.9% are achieved in 0.1 wt% and 0.2 wt% KDFP electrolyte. Importantly, the Coulombic efficiency of the subsequent cycles approaches 100% with KDFP addition (95.9 % for 0 wt % KDFP, 98.2 % for 0.1 wt% KDFP, and 99.8 % for 0.2 wt% KDFP in the second cycle), which also verifies the stable SEI formed in the presence of KDFP additive (see **Table S3** for comparison). Likewise, the onset potential associated with the potassiation of graphite, shifts towards a more positive region and vice versa during depotassiation (see **Table S2** for comparison). This further corroborates the positive influence of KDFP in reducing the reaction overpotential. The more comprehensive (de)potassiation process exhibited in this case is as a result of a less resistive SEI film being formed in the presence of KDFP.[35]

As shown in **Figure S10** and summarized in **Tables S2** and **S3**, the addition of FEC does not substantially contribute to improvement in the electrochemical behavior of graphite electrodes. The overpotential of (de)potassiation even increases by adding FEC, implying that an inferior, non-protective SEI layer is formed from the decomposition of FEC. This finding corroborates a previous study whereby the graphite electrode in a KPF_6-based electrolyte with 3 wt% FEC could not withstand cycling over 3 times.[43] These results clearly suggest that some established additives used in LIBs may be ineffective or even detrimental in the PIBs.

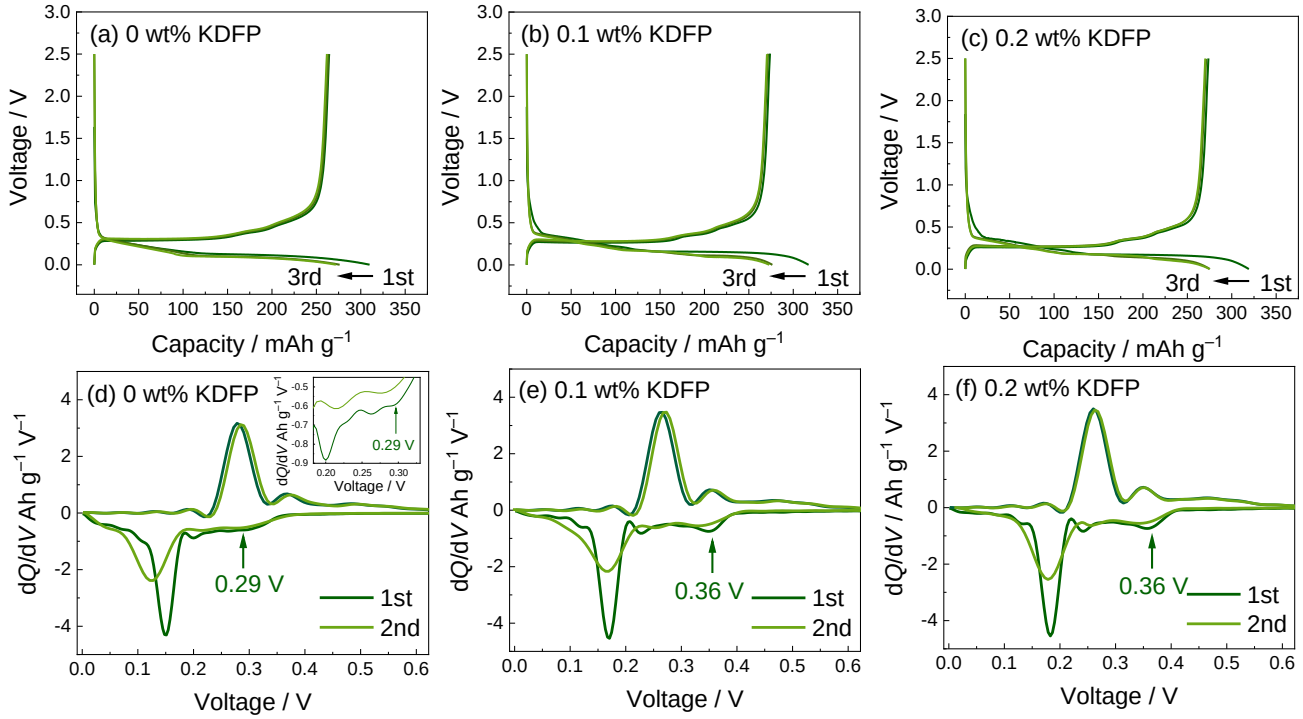

Figure 4. Charge-discharge curves of the K/graphite cells in 0.5 M KPF_6-EC/DEC with (a) 0 wt%, (b) 0.1 wt%, and (c) 0.2 wt% KDFP. Current density: C/20 (1C = 279 mA g^{-1}). The corresponding differential capacity vs. voltage (dQ/dV) plots of the first two charge-discharge cycles are shown in (d–f). (See **Figure S10** for charge-discharge curves and the corresponding dQ/dV plots of the ones with FEC additive. See **Table S2** for the peak position during potassiation and depotassiation of the initial cycle.)

The effect of the additives on the structural evolution of graphite electrodes undergoing (de)potassiation was further investigated through *ex-situ* XRD and Raman spectroscopic analysis. As illustrated in **Figure 5** and **Figure S12**, XRD patterns and Raman spectra of the pristine, fully charged, and fully discharged graphite electrodes in 0.5 M KPF_6-EC/DEC with 0 wt%, 0.1 wt%, and 0.2 wt% KDFP were obtained.

As can be seen in **Figure 5a**, a sharp peak corresponding to an interlayer distance of 3.36 Å appears at 26.46° on the 002 diffraction line of the pristine graphite electrode.[44] After charging the cell at C/20 to 0.001 V in the electrolyte without additive, the 002 peak disappears, and two characteristic peaks assignable to KC_8 appear at 16.4 (5.40 Å) and 33.3° (2.69 Å). The XRD reflections of K-GICs obey the (00*l*) plane along the *c*-axis giving an interlayer distance of 5.40 Å. In previous works on the stage-1 K-GIC (KC_8), two different indexing manners (001 and 002[21] or 004 and 008[6, 45]) were proposed for these peaks depending on the interlayer arrangements of K^+. In addition to the diffraction peaks of KC_8, a small peak assignable to the residual stage-2 K-GIC (KC_{24}) appears at 20.1°, indicating the incomplete potassiation of K-GIC. After discharging, the characteristic 002 peak of graphite is reformed but with a lower intensity and a broader shape; indicating the original layered structure is recovered but with a certain degree of damage caused by the volume variation. As shown in **Figure 5d**, the G band of the pristine graphite shifts from 1580 cm^{-1} to 1600 cm^{-1} after charging, confirming the existence of the residue of stage-2 K-GIC (KC_{24}) on the surface of charged graphite electrode (see the literature for assignments of the K-GIC Raman bands).[4, 21] The G and D bands of graphite which are also recovered after discharging, show consistency with the XRD results.

In the case of the 0.1 wt% KDFP electrolyte, the diffraction peak of KC_{24} disappears leaving only

the ones assigned to KC_8 in the charged electrode (**Figure S12a**). However, the corresponding Raman spectrum shows that a characteristic Fano-type band of KC_8 at 1430 cm^{-1} [46-47] appears alongside a band of KC_{24} on the high wavenumber side, implying that the stage-2 K-GIC still exists on the surface of the charged graphite electrode (**Figure S12b**).[48] Interestingly, when the KDFP concentration in the electrolyte increased to 0.2 wt%, phase-pure KC_8 could exclusively be formed after charging, with characteristic peaks appearing at 16.50° and 33.40°[22] (**Figure 5b**). Maximum intensity was observed on the typical KC_8 broad Fano-type band[46] at around 1430 cm^{-1} (**Figure 5e**). The complete and reversible formation of phase-pure KC_8 from the pristine graphite verified by these *ex-situ* analyses illustrates the best electrochemical performance[22] is attained with 0.2 wt% KDFP.

To gain deeper insight on the influence of the electrolyte additive on the (de)potassiation behavior of graphite, galvanostatic intermittent titration technique (GITT)[49] was employed to acquire charge/discharge profiles approaching to the thermodynamic equilibrium (**Figure S11a and S11b**). The evolution of the quasi-equilibrium voltage vs. time (dV/dt) is shown in **Figure S11c**. Since the steady-state of phase transformation occur in the voltage plateau, in theory, the voltage variation in this region should be zero. As can be seen, the measured dV/dt values remain constant at zero for a more prolonged state of (dis)charge in the case of 0.2 wt% KDFP than in the electrolyte without additive. This extended region of $dV/dt \approx 0$ indicates that for the selected electrode, a faster equilibrium is reached and favorable diffusion path in SEI layer is established with the aid of KDFP.

To draw a comparison, the (de)potassiation process of graphite in the FEC containing electrolyte has also been investigated by XRD and Raman analyses. As shown in **Figure 5c**, the potassiated graphite shows a pair of strong diffraction peaks of KC_{24} with even greater intensity than those of KC_8. The residual KC_{24} seen after discharge indicates the poor reversibility of (de)potassiation in the

electrolyte with FEC. These findings are further supported by the Raman spectra (**Figure 5f**). Thus, the rapid capacity fading of graphite in the FEC-added electrolyte can be attributed to the irreversibility of K-GIC staging process.

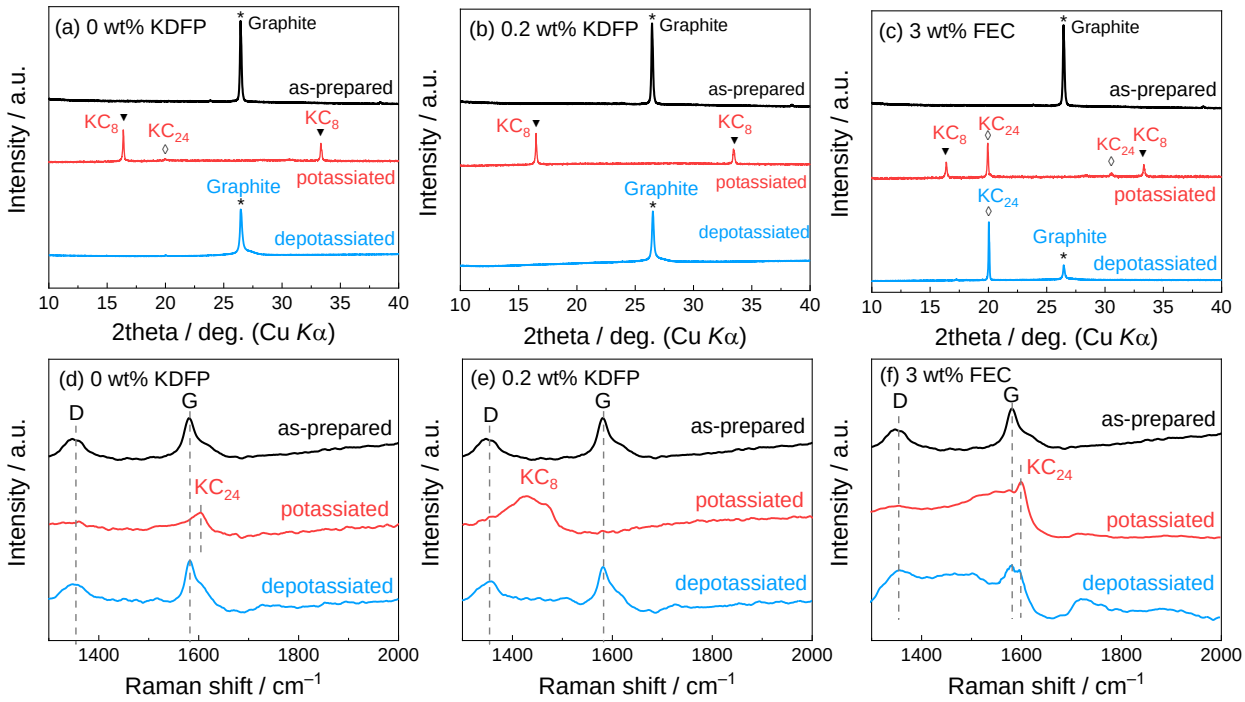

Figure 5. *Ex-situ* XRD patterns and Raman spectra of graphite electrodes at pristine (black), fully potassiated (red), and fully depotassiated (blue) states. Electrolytes: 0.5 M KPF_6-EC/DEC with (a, d) 0 wt%, (b, e) 0.2 wt% KDFP, and (c, f) 0.3 wt% FEC. (see Fig. S12 for XRD patterns and Raman spectra in the case with 0.1 wt% KDFP).

The rate performance of the K/graphite half-cell was further evaluated in the voltage range of 0.001–2.5 V at current densities of C/20, C/10, C/5, C/2, 1C, and C/20 at 25 °C as shown in **Figure S13**. The results show significant improvements in the rate capability with increasing concentration of KDFP. After cycling at different rates, a reversible capacity as high as 272 mAh g^{-1} could be obtained

from the electrolyte with 0.2 wt% KDFP at the current density of C/20. The corresponding charge-discharge curves shown in **Figure S14** clearly indicate diminished polarization with regards to the electrolyte with 0.2 wt% KDFP. This further substantiates the dQ/dV results (**Figure 4**) reported in this study and additionally highlights the positive influence of KDFP additive on (de)potassiation kinetics. The minimal deviation from the equilibrium voltage observed in the galvanostatic intermittent titration technique performed on cells containing the KDFP additive, also substantiates that the presence of KDFP is auspicious in the formation of a more ionically conductive SEI that leads to the better (de)potassiation kinetics observed. Similar findings have been made in corresponding studies on the lithium analog, LiDFP, indicating enhanced rate capability in the performance of graphite electrodes for LIBs [33, 35].

Figure 6a shows the cycle performance of K/graphite half-cells with varying amounts of KDFP evaluated in the voltage range of 0.001–2.5 V at a current density of C/3 and temperature of 25 °C. As can be seen, the capacity of the cell without KDFP dramatically decays after 40 cycles exhibiting low capacity retention (27.4%) at the 100th cycle (discharge capacity of 56 mAh g^{-1}). In contrast, the cells containing the KDFP additive manifested significant enhancement in the cycling stability and discharge capacity retention. In particular, the discharge capacity retention of the cell with 0.2 wt% KDFP is 89.0% at the 100th cycle and 76.8% at the 400 cycles (discharge capacity: 181 mAh g^{-1}). Furthermore, the comparison of Coulombic efficiencies of the cells with and without KDFP over the initial 15 cycles presented in **Figure 6b** shows that cells consisting of electrolytes with the additive need fewer cycles to achieve a Coulombic efficiency ≥ 99.9%, exemplifying the formation of stable SEI film. These results clearly affirm the importance of adopting a suitable electrolyte additive for feasible PIB operations.

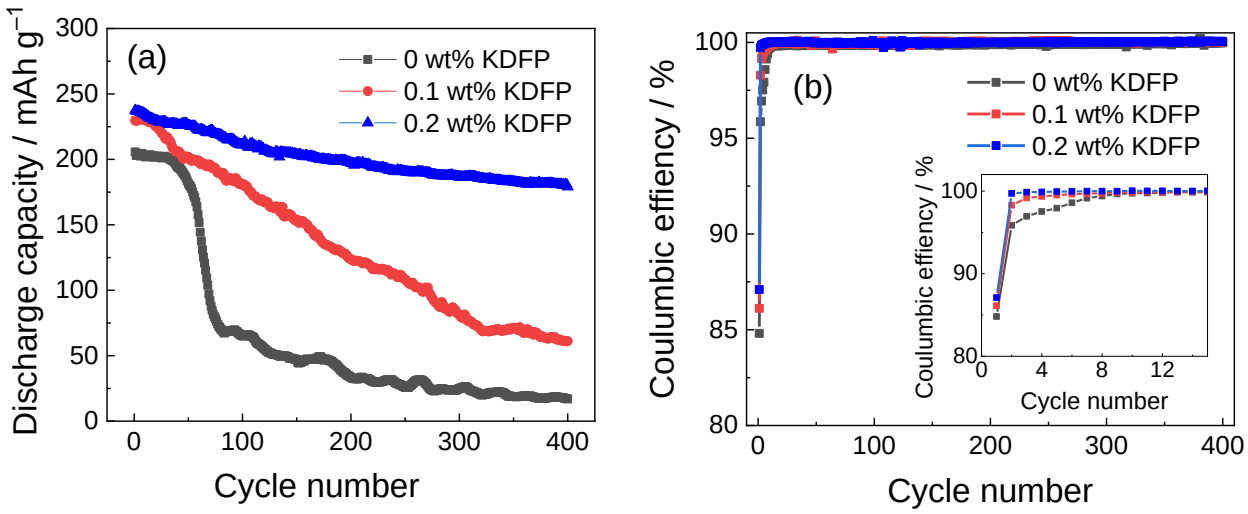

Figure 6. Cycle performance of the K/graphite cells with 0.5 M KPF_6-EC/DEC with 0 wt%, 0.1 wt%, and 0.2 wt% of KDFP. (a) Capacity retention and (b) Coulombic efficiency. C-rate: C/3. Cut-off voltage: 0.001–2.5 V.

The SEM images of the pristine graphite electrode and the ones after cycling are provided in **Figure S15**. **Figure S15a,b** shows the surface morphology of the pristine graphite particles with flake-like structures. After 400 cycles in the electrolyte without additive, a thick surface layer is formed on the graphite electrode (**Figure S15d**). In addition, the particle of graphite is partly exfoliated into a smaller size compared with the pristine graphite (**Figure S15c**). The graphite electrode with 0.2 wt% KDFP shows an evenly distributed SEI film which protects the flake-like structures of the graphite even after 400 cycles (**Figure S15e,f**). As shown in **Figure S15g,h**, a thick SEI film is deposited even after 3 cycles and blocks pores of the graphite electrode, which agrees with the severe degradation during cycling (**Figure S10b**). This phenomenon also provides an insight in the inferior electrochemical performance with FEC additive in KIB.

X-ray photoelectron spectroscopic analysis was carried out to ascertain the components of the SEI layer of graphite electrodes undergoing (de)potassiation and verify the possible effects of the additive on the electrochemical performance. **Figure 7** shows K 2p, C 1s, O 1s, F 1s, and P 2p XPS spectra of graphite electrodes after 400 cycles in 0.5 M KPF_6-EC/DEC with 0 wt% and 0.2 wt% KDFP (see **Table S4** for assignments). For the pristine graphite electrode, the characteristic peaks in the C 1s spectrum appearing at 284.4 eV and 285.3 eV can be assigned to be sp^2 and sp^3 carbon, respectively. The peak appearing at 290.9 eV in C 1s is considered to be indicative of π–π* transition (**Figure S16**).[50] Partially oxidized graphite which results in weak peaks at 286.1 eV for C–O (also from CMC binder) and 287.2 eV for C=O, is also consistently observed in the O 1s spectra at 533.6 eV for C–O and 532.1 eV for C=O.[23, 51] Graphite electrodes cycled in both the electrolytes with and without the KDFP additive, showed significant increases in the intensities of C–O, C=O, and -CO_3^{2-} peaks in the C 1s spectra (**Figure 7a**), and the K–O species are observable at 528.8 eV in the O 1s spectra (**Figure 7b**).[52] [53] These results validate the formation of the SEI layer by electrolyte decomposition and shows good agreement with previous works for potassium-ion batteries with KPF_6 electrolyte.[23, 51-53]

The main difference in the SEI constituents formed by electrolytes with and without additive can be observed in the F 1s and P 2p spectra. In both the electrolytes, the presence of CF_x, PF_x species (687.5 ± 1 eV), and KF (683.6 eV) are confirmed in F 1s spectra.[52] However, the KF ratio increases from 15.1% to 25.1 % in the presence of 0.2 wt% KDFP (**Figure 7c**), in conformity with previous reports on the effect of LiDFP additive in LIBs.[35] Although, KF species can be detected in the K metal counter electrode recovered from the electrolyte with 0.2 wt% KDFP, they are not detected in the electrolyte without the additive (**Figure S16c**). Additional evidence of the distinctive SEI formed by the addition of KDFP is also furnished by the P 2p spectra as illustrated in **Figure 7d**. Two peaks

associated with K_xPF_y and phosphate (PO_x), are observed at 137.7 eV and 133.7 eV respectively. On the other hand, the spectrum of the electrode cycled in the electrolyte with 0 wt% KDFP shows only one peak of K_xPF_y at 137.6 eV. It can, therefore, be inferred that these phosphate species are created through the addition of KDFP into the electrolyte. According to the previous studies on the use of LiDFP additive in LIB electrolytes, phosphate species are considered to be favorable components of SEI during interfacial reactions and Li^+ diffusion.[35] In a similar manner, it is expected that the addition of KDFP could promote the formation of a stable and more ionically conductive SEI layer, which contributes to the facile reaction in the K/K symmetric and K/graphite cells observed in this system.

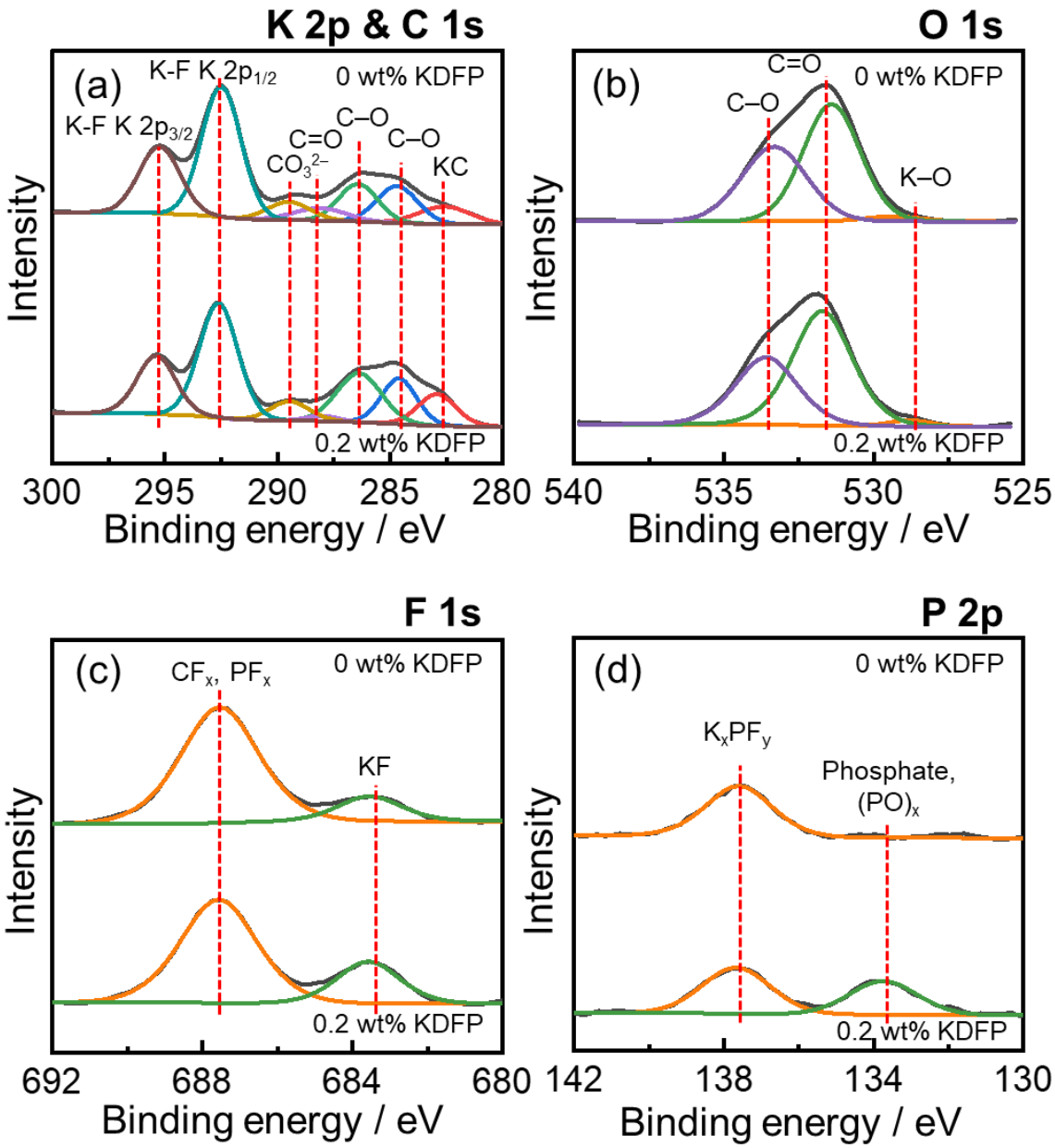

Figure 7. X-ray photoelectron spectra of SEI layers formed on graphite electrodes after 400 cycles in 0.5 M KPF_6 EC/DEC with and without KDFP additive in the (a) K 2p and C 1s, (b) O 1s, (c) F 1s, and (d) P 2p regions. (See **Table S4** for the binding energy of the peaks and SEI components and **Figure S16** for the XPS spectra of pristine graphite electrode and K metal electrode after 400 cycles.)

4. Conclusions

In conclusion, the feasibility of KDFP additive in KPF_6-based electrolytes has been systematically investigated using K metal and graphite electrodes. Potassium metal deposition/dissolution tests and EIS measurements confirmed that a stable SEI with improved ionic conductivity is formed on the electrode surface during operation in the electrolyte containing KDFP. Furthermore, a high discharge capacity of 274 mAh g^{-1} (98.2% of the theoretical value) was achieved from graphite electrodes in the electrolyte with 0.2 wt% KDFP as a result of the complete and reversible formation of phase-pure stage-1 K-GIC (KC_8). The electrolyte containing KDFP is also seen to significantly improve the rate performance and cyclability of graphite, delivering a 76.8% capacity retention after 400 cycles with an averaged Coulombic efficiency of 99.9%. It is important to note that such improvements could not be attained when FEC (another common additive) was used instead; attesting to the unique role of KDFP. Additional XPS analysis performed on the graphite electrodes after cycling in the electrolyte containing KDFP indicated that enriched KF and PO_x species were formed in the SEI layer, causing the improved interfacial properties and the diminished (de)potassiation overpotential. This study not only demonstrates a simple and effective way to acquire stage-1 K-GIC from high performance PIB electrolytes but also establishes the use of small amounts additives as a judicious way to boost the electrochemical performance of certain electrode materials.

ASSOCIATED CONTENT

Supporting Information (PDF)

Supporting Information is available free of charge on the ACS Publications website at DOI: XXXXXXX.

Structure and physical (viscosity, ionic conductivity) data, electrochemical measurement data, and analytical data by XRD and Raman and XPS spectroscopies.

AUTHOR INFORMATION

Corresponding Author

E-mail: k-matsumoto@energy.kyoto-u.ac.jp (K.M.).

Notes

The authors declare no competing financial interest.

ORCID

Huan Yang: 0000-0002-8757-5733

Chih-yao Chen: 0000-0002-8799-4647

Jinkwang Hwang: 0000-0003-4800-3158

Keigo Kubota: 0000-0002-0536-129X

Kazuhiko Matsumoto: 0000-0002-0770-9210

Rika Hagiwara: 0000-0002-7234-3980

ACKNOWLEDGMENT

This study was partly supported by the Japanese Ministry of Education, Culture, Sports, Science and Technology (MEXT) program “Elements Strategy Initiative to Form Core Research Center” (JPMXP0112101003) and Japan Society for the Promotion of Science (JSPS) KAKENHI Grant Number 19H04695. One of the authors, H. Y., thanks to China Scholarship Council (CSC) for their financial support.

5. References

1. Tarascon, J.-M., Is Lithium the New Gold? *Nat. Chem.* **2010**, *2*, 510.

2. Larcher, D.; Tarascon, J.-M., Towards Greener and More Sustainable Batteries for Electrical Energy Storage. *Nat. Chem.* **2015**, *7*, 19-29.

3. Matsumoto, K.; Hwang, J.; Kaushik, S.; Chen, C.-Y.; Hagiwara, R., Advances in Sodium Secondary Batteries Utilizing Ionic Liquid Electrolytes. *Energy Environ. Sci.* **2019**, *12*, 3247-3287.

4. Luo, W.; Wan, J.; Ozdemir, B.; Bao, W.; Chen, Y.; Dai, J.; Lin, H.; Xu, Y.; Gu, F.; Barone, V., Potassium Ion Batteries with Graphitic Materials. *Nano Lett.* **2015**, *15*, 7671-7677.

5. Lei, K.; Li, F.; Mu, C.; Wang, J.; Zhao, Q.; Chen, C.; Chen, J., High K-Storage Performance Based on the Synergy of Dipotassium Terephthalate and Ether-Based Electrolytes. *Energy Environ. Sci.* **2017**, *10*, 552-557.

6. Komaba, S.; Hasegawa, T.; Dahbi, M.; Kubota, K., Potassium Intercalation into Graphite to Realize High-Voltage/High-Power Potassium-Ion Batteries and Potassium-Ion Capacitors. *Electrochem. Commun.* **2015**, *60*, 172-175.

7. Fan, L.; Ma, R.; Wang, J.; Yang, H.; Lu, B., An Ultrafast and Highly Stable Potassium–Organic Battery. *Adv. Mater.* **2018**, *30*, 1805486.

8. Fan, L.; Lin, K.; Wang, J.; Ma, R.; Lu, B., A Nonaqueous Potassium‐Based Battery‐Supercapacitor Hybrid Device. *Adv. Mater.* **2018**, *30*, 1800804.

9. Fan, L.; Chen, S.; Ma, R.; Wang, J.; Wang, L.; Zhang, Q.; Zhang, E.; Liu, Z.; Lu, B., Ultrastable Potassium Storage Performance Realized by Highly Effective Solid Electrolyte Interphase Layer. *Small* **2018**, *14*, 1801806.

10. Liu, S.; Mao, J.; Zhang, Q.; Wang, Z.; Pang, W. K.; Zhang, L.; Du, A.; Sencadas, V.; Zhang, W.;

Guo, Z., An Intrinsically Non‐Flammable Electrolyte for High‐Performance Potassium Batteries. *Angew. Chem., Int. Ed.* **2020**, *59*, 3638-3644.

11. Matsuda, Y.; Nakashima, H.; Morita, M.; Takasu, Y., Behavior of Some Ions in Mixed Organic Electrolytes of High Energy Density Batteries. *J. Electrochem. Soc.* **1981**, *128*, 2552-2556.

12. Wang, L.; Yang, J.; Li, J.; Chen, T.; Chen, S.; Wu, Z.; Qiu, J.; Wang, B.; Gao, P.; Niu, X., Graphite as a Potassium Ion Battery Anode in Carbonate-Based Electrolyte and Ether-Based Electrolyte. *J. Power Sources* **2019**, *409*, 24-30.

13. Li, Y.; Lu, Y.; Adelhelm, P.; Titirici, M.-M.; Hu, Y.-S., Intercalation Chemistry of Graphite: Alkali Metal Ions and Beyond. *Chem. Soc. Rev.* **2019**, *48*, 4655-4687.

14. Yoon, G.; Kim, H.; Park, I.; Kang, K., Conditions for Reversible Na Intercalation in Graphite: Theoretical Studies on the Interplay among Guest Ions, Solvent, and Graphite Host. *Adv. Energy Mater.* **2017**, *7*, 1601519.

15. Wen, Y.; He, K.; Zhu, Y.; Han, F.; Xu, Y.; Matsuda, I.; Ishii, Y.; Cumings, J.; Wang, C., Expanded Graphite as Superior Anode for Sodium-Ion Batteries. *Nat. Commun.* **2014**, *5*, 1-10.

16. Goktas, M.; Bolli, C.; Berg, E. J.; Novák, P.; Pollok, K.; Langenhorst, F.; Roeder, M. v.; Lenchuk, O.; Mollenhauer, D.; Adelhelm, P., Graphite as Cointercalation Electrode for Sodium-Ion Batteries: Electrode Dynamics and the Missing Solid Electrolyte Interphase (SEI). *Adv. Energy Mater.* **2018**, *8*, 1702724.

17. Jache, B.; Adelhelm, P., Use of Graphite as a Highly Reversible Electrode with Superior Cycle Life for Sodium-Ion Batteries by Making Use of Co-Intercalation Phenomena. *Angew. Chem. Int. Ed.* **2014**, *53*, 10169-10173.

18. Ebert, L. B., Intercalation Compounds of Graphite. *Annu. Rev. Mater. Sci.* **1976**, *6*, 181-211.

19. Dresselhaus, M. S.; Dresselhaus, G., Intercalation Compounds of Graphite. *Adv. Phys.* **2002**, *51*, 1-186.

20. Enoki, T.; Suzuki, M.; Endo, M., *Graphite Intercalation Compounds and Applications*; Oxford University Press, 2003.

21. Liu, J.; Yin, T.; Tian, B.; Zhang, B.; Qian, C.; Wang, Z.; Zhang, L.; Liang, P.; Chen, Z.; Yan, J., Unraveling the Potassium Storage Mechanism in Graphite Foam. *Adv. Energy Mater.* **2019**, *9*, 1900579.

22. Jian, Z.; Luo, W.; Ji, X., Carbon Electrodes for K-Ion Batteries. *J. Am. Chem. Soc* **2015**, *137*, 11566-11569.

23. Fan, L.; Ma, R.; Zhang, Q.; Jia, X.; Lu, B., Graphite Anode for Potassium Ion Battery with Unprecedented Performance. *Angew. Chem., Int. Ed.* **2019**, *58*, 10500 –10505.

24. Pramudita, J. C.; Peterson, V. K.; Kimpton, J. A.; Sharma, N., Potassium-Ion Intercalation in Graphite within a Potassium-Ion Battery Examined Using in Situ X-Ray Diffraction. *Powder Diffr.* **2017**, *32*, S43-S48.

25. Zhao, J.; Zou, X.; Zhu, Y.; Xu, Y.; Wang, C., Electrochemical Intercalation of Potassium into Graphite. *Adv. Funct. Mater.* **2016**, *26*, 8103-8110.

26. Rajagopalan, R.; Tang, Y.; Ji, X.; Jia, C.; Wang, H., Advancements and Challenges in Potassium Ion Batteries: A Comprehensive Review. *Adv. Funct. Mater.* **2020**, 1909486.

27. Wei, S.; Choudhury, S.; Tu, Z.; Zhang, K.; Archer, L. A., Electrochemical Interphases for High-Energy Storage Using Reactive Metal Anodes. *Acc. Chem. Res.* **2018**, *51*, 80-88.

28. Mai, S.; Xu, M.; Liao, X.; Hu, J.; Lin, H.; Xing, L.; Liao, Y.; Li, X.; Li, W., Tris (Trimethylsilyl) Phosphite as Electrolyte Additive for High Voltage Layered Lithium Nickel Cobalt Manganese Oxide Cathode of Lithium Ion Battery. *Electrochim. Acta* **2014**, *147*, 565-571.

29. Self, J.; Hall, D. S.; Madec, L.; Dahn, J., The Role of Prop-1-ene-1, 3-sultone as an Additive in Lithium-Ion Cells. *J. Power Sources* **2015**, *298*, 369-378.

30. Zuo, X.; Zhao, M.; Ma, X.; Xiao, X.; Liu, J.; Nan, J., Effect of Diphenyl Disulfide as an Additive on the Electrochemical Performance of $Li_{1.2}Mn_{0.54}Ni_{0.13}Co_{0.13}O_2$/Graphite Batteries at Elevated Temperature. *Electrochim. Acta* **2017**, *245*, 705-714.

31. Zhang, H.; Feng, W.; Nie, J.; Zhou, Z., Recent Progresses on Electrolytes of Fluorosulfonimide Anions for Improving the Performances of Rechargeable Li and Li-Ion Battery. *J. Fluorine Chem.* **2015**, *174*, 49-61.

32. Song, Y.-M.; Kim, C.-K.; Kim, K.-E.; Hong, S. Y.; Choi, N.-S., Exploiting Chemically and Electrochemically Reactive Phosphite Derivatives for High-Voltage Spinel $LiNi_{0.5}Mn_{1.5}O_4$ Cathodes. *J. Power Sources* **2016**, *302*, 22-30.

33. Yang, B.; Zhang, H.; Yu, L.; Fan, W.; Huang, D., Lithium Difluorophosphate as an Additive to Improve the Low Temperature Performance of $LiNi_{0.5}Co_{0.2}Mn_{0.3}O_2$/Graphite Cells. *Electrochim. Acta* **2016**, *221*, 107-114.

34. Yang, G.; Shi, J.; Shen, C.; Wang, S.; Xia, L.; Hu, H.; Luo, H.; Xia, Y.; Liu, Z., Improving the Cyclability Performance of Lithium-Ion Batteries by Introducing Lithium Difluorophosphate ($LiPO_2F_2$) Additive. *RSC Adv.* **2017**, *7*, 26052-26059.

35. Kim, K.-E.; Jang, J. Y.; Park, I.; Woo, M.-H.; Jeong, M.-H.; Shin, W. C.; Ue, M.; Choi, N.-S., A Combination of Lithium Difluorophosphate and Vinylene Carbonate as Reducible Additives to Improve Cycling Performance of Graphite Electrodes at High Rates. *Electrochem. Commun.* **2015**, *61*, 121-124.

36. Matsumoto, K.; Hagiwara, R., A New Series of Ionic Liquids Based on the Difluorophosphate

Anion. *Inorg. Chem.* **2009**, *48*, 7350-7358.

37. Wang, C.; Yu, L.; Fan, W.; Liu, J.; Ouyang, L.; Yang, L.; Zhu, M., Lithium Difluorophosphate as a Promising Electrolyte Lithium Additive for High-Voltage Lithium-Ion Batteries. *ACS Appl. Energy Mater.* **2018**, *1*, 2647-2656.

38. Yang, H.; Hwang, J.; Wang, Y.; Matsumoto, K.; Hagiwara, R., N-Ethyl-N-Propylpyrrolidinium Bis (Fluorosulfonyl) Amide Ionic Liquid Electrolytes for Sodium Secondary Batteries: Effects of Na Ion Concentration. *J. Phys. Chem. C* **2019**, *123*, 22018-22026.

39. Hwang, J.; Okada, H.; Haraguchi, R.; Tawa, S.; Matsumoto, K.; Hagiwara, R., Ionic Liquid Electrolyte for Room to Intermediate Temperature Operating Li Metal Batteries: Dendrite Suppression and Improved Performance. *J. Power Sources* **2020**, *453*, 227911.

40. Iermakova, D.; Dugas, R.; Palacín, M.; Ponrouch, A., On the Comparative Stability of Li and Na Metal Anode Interfaces in Conventional Alkyl Carbonate Electrolytes. *J. Electrochem. Soc.* **2015**, *162*, A7060-A7066.

41. Forsyth, M.; Yoon, H.; Chen, F.; Zhu, H.; MacFarlane, D. R.; Armand, M.; Howlett, P. C., Novel Na^+ Ion Diffusion Mechanism in Mixed Organic-Inorganic Ionic Liquid Electrolyte Leading to High Na^+ Transference Number and Stable, High Rate Electrochemical Cycling of Sodium Cells. *J. Phys. Chem. C* **2016**, *120*, 4276-4286.

42. Hwang, J.; Matsumoto, K.; Hagiwara, R., $Na_3V_2(PO_4)_3$/C Positive Electrodes with High Energy and Power Densities for Sodium Secondary Batteries with Ionic Liquid Electrolytes That Operate across Wide Temperature Ranges. *Adv. Sustainable Syst.* **2018**, *2*, 1700171.

43. Bie, X.; Kubota, K.; Hosaka, T.; Chihara, K.; Komaba, S., A Novel K-Ion Battery: Hexacyanoferrate (II)/Graphite Cell. *J. Mater. Chem. A* **2017**, *5*, 4325-4330.

44. Eckmann, A.; Felten, A.; Mishchenko, A.; Britnell, L.; Krupke, R.; Novoselov, K. S.; Casiraghi, C., Probing the Nature of Defects in Graphene by Raman Spectroscopy. *Nano Lett.* **2012**, *12*, 3925-3930.

45. Rüdorff, W.; Schulze, E., Über Alkaligraphitverbindungen. *Zeitschrift für anorganische und allgemeine Chemie* **1954**, *277*, 156-171.

46. Ichimura, K.; Takamura, E.; Sano, M., Hydrogen in Alkali-Metal-Graphite Intercalation Compounds. *Synth. Met.* **1991**, *40*, 355-368.

47. Nemanich, R.; Solin, S.; Guerard, D., Raman Scattering from Intercalated Donor Compounds of Graphite. *Phys. Rev. B* **1977**, *16*, 2965-2972.

48. Purewal, J. Hydrogen Adsorption by Alkali Metal Graphite Intercalation Compounds. California Institute of Technology, 2010.

49. Tang, K.; Yu, X.; Sun, J.; Li, H.; Huang, X., Kinetic Analysis on $LiFePO_4$ Thin Films by CV, GITT, and EIS. *Electrochim. Acta* **2011**, *56*, 4869-4875.

50. Sette, F.; Wertheim, G.; Ma, Y.; Meigs, G.; Modesti, S.; Chen, C., Lifetime and Screening of the C 1s Photoemission in Graphite. *Phys. Rev. B* **1990**, *41*, 9766-9770.

51. Zhang, Q.; Mao, J.; Pang, W. K.; Zheng, T.; Sencadas, V.; Chen, Y.; Liu, Y.; Guo, Z., Boosting the Potassium Storage Performance of Alloy-Based Anode Materials Via Electrolyte Salt Chemistry. *Adv. Energy Mater.* **2018**, *8*, 1703288.

52. Lei, Y.; Han, D.; Dong, J.; Qin, L.; Li, X.; Zhai, D.; Li, B.; Wu, Y.; Kang, F., Unveiling the Influence of Electrode/Electrolyte Interface on the Capacity Fading for Typical Graphite-Based Potassium-Ion Batteries. *Energy Storage Mater.* **2020**, *24*, 319-328.

53. Wang, H.; Hu, J.; Dong, J.; Lau, K. C.; Qin, L.; Lei, Y.; Li, B.; Zhai, D.; Wu, Y.; Kang, F.,

Potassium Metal Batteries: Artificial Solid-Electrolyte Interphase Enabled High-Capacity and Stable Cycling Potassium Metal Batteries. *Adv. Energy Mater.* **2019**, *9*, 1970168.

Graphical abstract